SIAM J. NUMER. ANAL.
Vol. 36, No. 1, pp. 251–274

THE ADAPTIVE COMPUTATION OF FAR-FIELD PATTERNS BY A POSTERIORI ERROR ESTIMATION OF LINEAR FUNCTIONALS*

PETER MONK† AND ENDRE SÜLI‡

Abstract. This paper is concerned with the derivation of a priori and a posteriori error bounds for a class of linear functionals arising in electromagnetics which represent the far-field pattern of the scattered electromagnetic field. The a posteriori error bound is implemented into an adaptive finite element algorithm, and a series of numerical experiments is presented.

Key words. linear functional, far field, a posteriori error estimates

AMS subject classifications. 35J20, 65N15, 65N30

PII. S0036142997315172

1. Introduction.

In many physical phenomena modeled by partial differential equations, the key quantity of concern is a certain linear functional $N(u)$ of the underlying solution u to the differential equation, rather than u itself. For example, in fluid dynamics one is frequently interested in calculating the lift and drag coefficients of a body immersed in a viscous incompressible fluid whose flow is governed by the Navier–Stokes equations. The lift and drag coefficients are defined as integrals, over the boundary of the body, of the normal and tangential components of the stress tensor, respectively. Similarly, in elasticity theory, the main quantities of interest are the stress at selected points, the stress intensity factor, or the moments in shell and plate theory; these are all functionals of the underlying solution. In acoustic and electromagnetic theory the quantity of interest is often the far-field pattern.

A possible approach to constructing an accurate finite element approximation $N(u_h)$ to a bounded linear functional $N(u)$ is based on exploiting an adaptive finite element algorithm, driven by an a posteriori bound on the global error $\|u - u_h\|$ in a norm $\|\cdot\|$ in which the functional $N(\cdot)$ is bounded. Unfortunately, such a procedure will, almost inevitably, lead to a gross overestimate of the error $N(u) - N(u_h)$, which will result in an inefficient adaptive algorithm. It is, therefore, of interest to devise a more direct approach.

While for problems in structural mechanics there has been a considerable amount of work on extracting accurate approximations to relevant functionals of the solution by means of the finite element method (see, for example, Babuška and Miller [2, 3, 4] and the review article of Babuška and Suri [5]), these techniques have not penetrated the field of acoustics and electromagnetics; even for lift and drag problems in fluid

*Received by the editors January 20, 1997; accepted for publication (in revised form) January 6, 1998; published electronically December 2, 1998. The views and conclusions contained herein are those of the authors and should not be interpreted as necessarily representing the official policies or endorsements, either expressed or implied, of the Air Force Office of Scientific Research or the U.S. Government.

http://www.siam.org/journals/sinum/36-1/31517.html

†Department of Mathematical Sciences, University of Delaware, Newark DE 19716 (monk@math.udel.edu). The work of this author was sponsored by the Air Force Office of Scientific Research, Air Force Materials Command, USAF, under grant F49620-95-1-0067 and was carried out during a visit to Project ONDES at INRIA, France.

‡Oxford University Computing Lab., Wolfson Building, Parks Road, Oxford OX1 3QD, England (Endre.Suli@comlab.ox.ac.uk).

dynamics, tools of this kind have been developed and analyzed only very recently [14]. The approach advocated in those articles (usually attributed to Wheeler [24]) is based on modifying the finite element test space; see also Barrett and Elliott [7] for an a priori error analysis of this extraction method in the case of a linear elliptic convection-diffusion equation, and Ainsworth et al. [1] for an application of the technique to a nonlinear diffusion equation. Stimulated by those articles, the objective of the present paper is to develop an a posteriori error analysis for finite element approximations of a functional arising in electromagnetics that represents the far-field pattern of the scattered electromagnetic field.

In this paper we analyze the model problem of the scattering of a transverse time harmonic electromagnetic wave from a perfectly conducting infinite cylinder in which the magnetic field is polarized parallel to the axis of the cylinder. In this case the problem can be reduced to a scalar problem in two space dimensions. We suppose that the cross section of the cylinder occupies a smooth bounded region D in the plane (such that $\mathbb{R}^2 \setminus \overline{D}$ is connected) with boundary $\Gamma_s = \partial D$. Let the wavenumber of the radiation be denoted by the real positive number k. The normalized scattered magnetic field H (the component of the field parallel to the axis of the cylinder) satisfies the Helmholtz equation in $\mathbb{R}^2 \setminus \overline{D}$ together with an inhomogeneous Neumann condition on the scatterer due to the incident radiation. Finally, a radiation condition at infinity completes the equations, which are as follows:

$$\Delta H + k^2 H = 0 \quad \text{in } \mathbb{R}^2 \setminus \overline{D}, \tag{1a}$$

$$\frac{\partial H}{\partial \nu} = g \quad \text{on } \Gamma_s, \tag{1b}$$

$$\lim_{r\to\infty} \sqrt{r}\left(\frac{\partial H}{\partial r} - ikH\right) = 0, \tag{1c}$$

where $r = |\boldsymbol{x}|$ is the radial coordinate, ν is the inward unit normal to D, and g is a given function.

It can be shown (see, for example, [13]) that the solution of this problem has the following asymptotic expansion for large r:

$$H(\boldsymbol{x}) = \frac{\exp(ikr)}{\sqrt{r}}\left(H_\infty(\hat{\boldsymbol{x}}) + O\left(\frac{1}{r}\right)\right) \text{ as } r \to \infty,$$

where $\hat{\boldsymbol{x}} = \boldsymbol{x}/r$. In many applications the quantity of interest is the function H_∞, which is called the far-field pattern of the scattered field (this can be used to calculate the radar cross section, for example). Assuming that H is known in the neighborhood of a simple Lipschitz-smooth closed curve Γ_c containing the scatterer, it can be shown that

$$H_\infty(\hat{\boldsymbol{x}}) = \frac{\exp(i\pi/4)}{\sqrt{8\pi k}} \int_{\Gamma_c} \left\{ H(\boldsymbol{y}) \frac{\partial \exp(-ik\hat{\boldsymbol{x}}\cdot\boldsymbol{y})}{\partial \nu(\boldsymbol{y})} - \frac{\partial H}{\partial \nu(\boldsymbol{y})} \exp(-ik\hat{\boldsymbol{x}}\cdot\boldsymbol{y}) \right\} ds(\boldsymbol{y}), \tag{2}$$

where ν is the unit outward normal to Γ_c (i.e., ν points into the infinite region). The curve Γ_c is sometimes called a collection curve. In this paper we shall assume that Γ_c is chosen to be the boundary of a polygon (such as a rectangle). We shall also comment on the use of curvilinear collection surfaces such as circles or ellipses.

From (2) we can see that for each $\hat{\boldsymbol{x}}$, the far field is a simple linear functional of the magnetic field H.

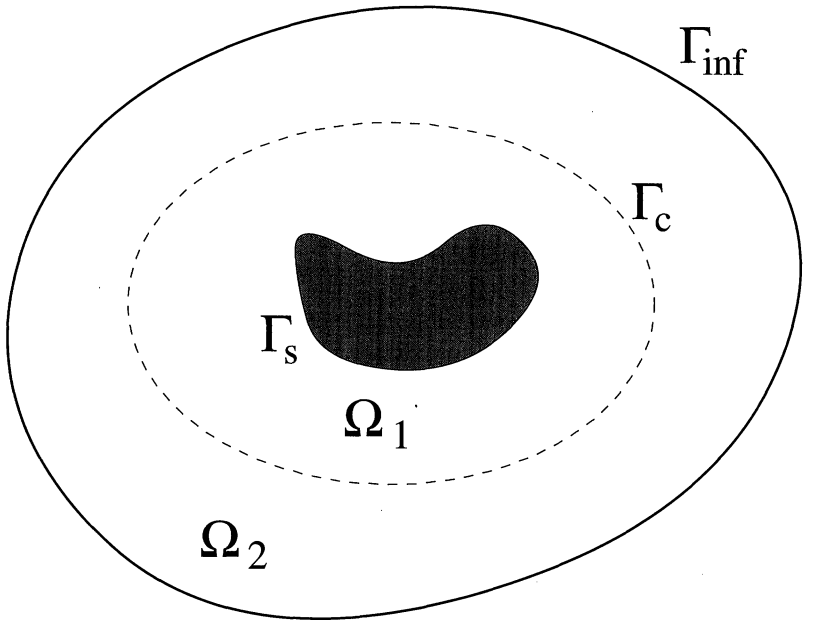

FIG. 1. *The scatterer D is shown as a shaded region in this figure. The region Ω outside D and inside Γ_{inf} is further subdivided into two regions: Ω_1 inside the collection curve Γ_c and Ω_2 outside Γ_c.*

For later use we shall define the functions ϕ and ψ by

$$\phi(\hat{\boldsymbol{x}}, \boldsymbol{y}) = \frac{\exp(i\pi/4)}{\sqrt{8\pi k}} \frac{\partial \exp(-ik\hat{\boldsymbol{x}} \cdot \boldsymbol{y})}{\partial \nu(\boldsymbol{y})}, \tag{3a}$$

$$\psi(\hat{\boldsymbol{x}}, \boldsymbol{y}) = \frac{\exp(i\pi/4)}{\sqrt{8\pi k}} \exp(-ik\hat{\boldsymbol{x}} \cdot \boldsymbol{y}). \tag{3b}$$

A common way to approximate the scattering problem (1a)–(1c) by finite elements is to truncate the infinite region outside D. Inside the truncated region the usual Helmholtz equation is satisfied and a suitable boundary condition is placed on the outer boundary to try to take care of the part of the solution on the infinite region. The simplest such choice is motivated by the radiation condition (1c). To state the resulting problem, let G be a bounded domain with a simply connected, smooth boundary containing $\overline{D}$ and Γ_c in its interior. Let $\Gamma_{inf} = \partial G$ and let $\Omega = G \setminus \overline{D}$. The geometry of Ω is shown in Figure 1. Then the approximate magnetic field, now denoted u to distinguish it from the true field, satisfies

$$\Delta u + k^2 u = 0 \quad \text{in } \Omega, \tag{4a}$$

$$\frac{\partial u}{\partial \nu} = g \quad \text{on } \Gamma_s, \tag{4b}$$

$$\frac{\partial u}{\partial \nu} - iku = 0 \quad \text{on } \Gamma_{inf}. \tag{4c}$$

This problem has been extensively studied (see, for example, [15]) and it can be shown that if Γ_{inf} is sufficiently far from the scatterer, then u is a good approximation to H. Of course it is possible to be much more sophisticated in treating the outer boundary

using more exotic absorbing conditions [12], matched absorbing layers [8], series solutions [18, 19], or integral equations [17, 20]. These all have various disadvantages and advantages, but we shall use the simple version in (4a)–(4c) since we wish to focus on the far-field calculation.

Given a solution to (4a)–(4c) we can compute an approximate far field corresponding to u by using (2) so that

$$u_\infty(\hat{\boldsymbol{x}}) = \int_{\Gamma_c} \left\{ u(\boldsymbol{y})\phi(\hat{\boldsymbol{x}}, \boldsymbol{y}) - \frac{\partial u}{\partial \nu(\boldsymbol{y})}\psi(\hat{\boldsymbol{x}}, \boldsymbol{y}) \right\} ds(\boldsymbol{y}). \tag{5}$$

In this paper we shall simply assume that Γ_{inf} has been chosen sufficiently far from D so that u_∞ is a good enough approximation to H_∞ (of course the a posteriori estimation of this error would be very useful). So all that is needed is to approximate u_∞ to a desired degree of accuracy.

Now we can state precisely the problem we shall study in this paper. Given a finite element approximation to u, we wish to study the a priori and a posteriori error estimates for the problem of computing the far-field pattern. Of course, one way to attack this problem would be to use a priori and a posteriori estimates in a suitable norm to estimate the error in the far-field pattern, exploiting the boundedness of the functional $u \to u_\infty$ in this norm. We want to avoid this and develop a theory for the functional directly. This approach has the advantage of giving sharper estimates and a clearer picture of the error.

2. The weak problem and its discretization. In this section we start by describing the weak formulation of the problem outlined in the introduction. We then show how to compute the far-field integrals (5) in this case. Next we discuss the discretization of the problem and the computation of the discrete far-field pattern. To define the weak problem associated with (4a)–(4c) we recall that the space $H^1(\Omega)$ is the classical Sobolev space of functions with derivatives in $L^2(\Omega)$. The norm on this space is denoted $\|\cdot\|_{1,\Omega}$ and defined by

$$\|u\|_{1,\Omega}^2 = \int_\Omega |\nabla u|^2 + k^2|u|^2 \, dA.$$

The $L^2(\Omega)$ norm is denoted $\|\cdot\|_{0,\Omega}$. Anticipating our later needs, we define the domains Ω_1 and Ω_2 to be the parts of Ω inside and outside Γ_c, respectively (see Figure 1). We denote by $[v]$ the jump in the value of v across Γ_c so that if v is continuous in $\overline{\Omega}_1$ and $\overline{\Omega}_2$ and $\boldsymbol{x} \in \Gamma_c$,

$$[v](\boldsymbol{x}) = \lim_{\boldsymbol{y}\to\boldsymbol{x}, \boldsymbol{y}\in\Omega_2} v(\boldsymbol{y}) - \lim_{\boldsymbol{y}\to\boldsymbol{x}, \boldsymbol{y}\in\Omega_1} v(\boldsymbol{y}).$$

Now we define the bilinear form $a : H^1(\Omega) \times H^1(\Omega) \to \mathbb{C}$ by

$$a(v, w) = \int_{\Omega_1} \left(\nabla v \cdot \nabla w - k^2 vw\right) dA + \int_{\Omega_2} \left(\nabla v \cdot \nabla w - k^2 vw\right) dA - ik \int_{\Gamma_{inf}} vw \, ds$$

and the following bilinear form on $L^2(\Gamma_s) \times L^2(\Gamma_s)$ by

$$\langle u, v\rangle_{\Gamma_s} = \int_{\Gamma_s} uv \, ds.$$

This notation will also be used for duality pairings on Γ_s. Note that we have not included complex conjugation in these definitions.

The weak solution $u \in H^1(\Omega)$ of (4a)–(4c) satisfies

$$a(u, v) = \langle g, v \rangle_{\Gamma_s} \text{ for all } v \in H^1(\Omega). \tag{6}$$

This problem has a unique solution and the usual elliptic regularity results and regularity shift theorems apply. Because $u \in H^1(\Omega)$, the far-field integral (5) is not directly applicable. To handle this in a way that generalizes to the finite element solution we proceed as follows. Let v be any function such that

$$v|_{\Omega_1} \in H^1(\Omega_1), \qquad v|_{\Omega_2} \in H^1(\Omega_2), \qquad [v] = \psi \text{ on } \Gamma_c. \tag{7}$$

Then, if u is a strong solution of the scattering problem, integration by parts and use of (4a)–(4c) shows that

$$\begin{aligned} \int_{\Gamma_c} \frac{\partial u}{\partial \nu} \psi \, ds &= \int_{\Gamma_c} \frac{\partial u}{\partial \nu} [v] \, ds \\ &= -\int_{\partial\Omega_2} \frac{\partial u}{\partial \nu_2} v|_{\Omega_2} \, ds + \int_{\Gamma_{inf}} \frac{\partial u}{\partial \nu_2} v|_{\Omega_2} \, ds \\ &\quad - \int_{\partial\Omega_1} \frac{\partial u}{\partial \nu_1} v|_{\Omega_1} \, ds + \int_{\Gamma_s} \frac{\partial u}{\partial \nu_1} v|_{\Omega_1} ds \\ &= -a(u, v) + \langle v, g \rangle_{\Gamma_s}, \end{aligned}$$

where ν_1 and ν_2 are, respectively, the unit outward normals to Ω_1 and Ω_2; the integrals over Γ_c, Γ_s, $\partial\Omega_1$, $\partial\Omega_2$ are to be understood as duality pairings between the Sobolev spaces $H^{-1/2}(S)$ and $H^{1/2}(S)$, with $S = \Gamma_c$, Γ_s, Ω_1, Ω_2, respectively.

Thus we may write

$$u_\infty = \int_{\Gamma_c} u\phi \, ds + a(u, v) - \langle v, g \rangle_{\Gamma_s}, \tag{8}$$

with v an arbitrary function satisfying (7). Of course, to compute $u_\infty(\hat{\boldsymbol{x}})$ requires the use of a different v (and ϕ) for each $\hat{\boldsymbol{x}}$.

The expression (8) is well defined for any $u \in H^1(\Omega)$ and is independent of the choice of v since if $u_\infty^{(1)}$ is the far field for $v = v_1$ and $u_\infty^{(2)}$ is the far field for $v = v_2$ (with the same ϕ and ψ), then

$$u_\infty^{(1)} - u_\infty^{(2)} = a(u, v_1 - v_2) - \langle v_1 - v_2, g \rangle_{\Gamma_s}.$$

However, $v_1 - v_2 \in H^1(\Omega)$ (the jump across Γ_c cancels) and hence, using (6), $u_\infty^{(1)} - u_\infty^{(2)} = 0$. The use of expressions like (8) to compute far-field patterns is not new (see, for example, [21, 22]).

Now we present the finite element problem. Suppose that Ω is meshed using a regular finite element mesh with elements of maximum diameter h so that Γ_c lies exactly along mesh lines. The mesh is assumed to be regular. The need to fit Γ_c exactly is the reason for choosing Γ_c to be the boundary of a polygon. If a smooth collection curve is used, then our theory would require the use of curved elements to exactly fit this curve. For simple curves such as circles or ellipses we could use the method of Bernardi [9]. The boundaries Γ_s and Γ_{inf} do not have to be fitted exactly since the boundary conditions are natural there, although in this paper we shall also assume that these boundaries have been fitted using curved elements. We

let $S_h \subset H^1(\Omega)$ be a finite element space on this mesh (we will be more specific about properties of the space later).

The finite element problem is to find $u_h \in S_h$ such that

$$a(u_h, v_h) = \langle g, v_h \rangle_{\Gamma_s} \text{ for all } v_h \in S_h. \tag{9}$$

We have not been specific about the construction of S_h so far. At this stage it is sufficient to assume (see subsection 3.1) that the space S_h has been constructed so that for all h small enough there is a unique solution to the discrete problem.

Once u_h has been computed, the approximate far-field pattern can be computed by using the discrete analogue of (8). Because Γ_c lies along mesh lines, the restriction of functions in S_h to Γ_c induces a natural discrete space on Γ_c that we denote by $B_h \subset H^1(\Gamma_c)$. Let $\psi_h \in B_h$ be an approximation to ψ (later we will analyze how the error in this approximation propagates to the computed far-field pattern). The fact that Γ_c is the boundary of a polygon implies that B_h is a standard finite element space of piecewise polynomials. In addition, since Γ_c is fitted exactly, we can define finite element spaces on Ω_1 and Ω_2 by

$$S_h^{(1)} = \{w_h|_{\Omega_1} \mid w_h \in S_h\} \text{ and } S_h^{(2)} = \{w_h|_{\Omega_2} \mid w_h \in S_h\}.$$

Now let v_h be a finite element function such that

$$v_h|_{\Omega_1} \in S_h^{(1)}, \qquad v_h|_{\Omega_2} \in S_h^{(2)}, \qquad [v_h] = \psi_h \text{ on } \Gamma_c. \tag{10}$$

Then we define the discrete far-field pattern by

$$u_{\infty,h} = \int_{\Gamma_c} u_h \phi \, ds + a(u_h, v_h) - \langle v_h, g \rangle_{\Gamma_s}. \tag{11}$$

In the same way as for the continuous problem, this definition is independent of the choice of v_h (but it does depend on the choice of ψ_h). To see this, suppose $u_{\infty,h}^{(1)}$ corresponds to $v_h^{(1)}$ and $u_{\infty,h}^{(2)}$ corresponds to $v_h^{(2)}$. Then

$$u_{\infty,h}^{(1)} - u_{\infty,h}^{(2)} = a(u, v_h^{(1)} - v_h^{(2)}) - \langle v_h^{(1)} - v_h^{(2)}, g \rangle_{\Gamma_s},$$

but $v_h^{(1)} - v_h^{(2)} \in S_h$ (the jump across Γ_c cancels) and hence, by (9), $u_{\infty,h}^{(1)} = u_{\infty,h}^{(2)}$.

3. A priori and a posteriori error analysis. The main theorem of this section is an exact characterization of the difference between u_∞ and $u_{\infty,h}$. From this characterization we can prove either a priori or a posteriori error estimates. To state the theorem we need the following auxiliary functions. Let ξ be the weak solution of the following problem:

$$\Delta \xi + k^2 \xi = 0 \text{ in } \Omega_1, \tag{12a}$$

$$\Delta \xi + k^2 \xi = 0 \text{ in } \Omega_2, \tag{12b}$$

$$[\xi] = \psi - \psi_h \text{ on } \Gamma_c, \tag{12c}$$

$$\left[\frac{\partial \xi}{\partial \nu}\right] = 0 \text{ on } \Gamma_c, \tag{12d}$$

$$\frac{\partial \xi}{\partial \nu} = 0 \text{ on } \Gamma_s, \tag{12e}$$

$$\frac{\partial \xi}{\partial \nu} - ik\xi = 0 \text{ on } \Gamma_{inf}, \tag{12f}$$

where $\psi_h \in B_h$ is an approximation to ψ. In subsection A.1, the regularity, existence, and uniqueness of the solution of this problem are analyzed.

Let z be the weak solution of the following problem:

$$\Delta z + k^2 z = 0 \text{ in } \Omega_1, \tag{13a}$$

$$\Delta z + k^2 z = 0 \text{ in } \Omega_2, \tag{13b}$$

$$[z] = f \text{ on } \Gamma_c, \tag{13c}$$

$$\left[\frac{\partial z}{\partial \nu}\right] = \phi \text{ on } \Gamma_c, \tag{13d}$$

$$\frac{\partial z}{\partial \nu} = 0 \text{ on } \Gamma_s, \tag{13e}$$

$$\frac{\partial z}{\partial \nu} - ikz = 0 \text{ on } \Gamma_{inf}, \tag{13f}$$

where $f \in H^{1/2}(\Gamma_c)$ will be chosen differently when performing the a priori and a posteriori analyses. The existence, uniqueness, and regularity of this problem are also analyzed in subsection A.1.

THEOREM 3.1. *The following equality holds:*

$$u_\infty - u_{\infty,h} = -\langle g, \xi \rangle_{\Gamma_s} + a(u - u_h, v_h - z),$$

where $v_h \in S_h$ *is any function satisfying* (10) *and* z *satisfies* (13a)–(13f) *for any* $f \in H^{1/2}(\Gamma_c)$.

Proof. Using the definitions of u_∞ (see (8)) and $u_{\infty,h}$ (see (11)) we obtain

$$u_\infty - u_{\infty,h} = \int_{\Gamma_c} (u - u_h)\phi \, ds + a(u, v) - a(u_h, v_h) - \langle g, v - v_h \rangle_{\Gamma_s}. \tag{14}$$

Now we choose $v = v_h + \xi$. Note that $[v] = [v_h] + [\xi] = \psi_h + \psi - \psi_h = \psi$ so that v is a function satisfying (7). With this choice, and adding suitable terms to the left-hand side of (14), we obtain

$$\begin{aligned} u_\infty - u_{\infty,h} &= \int_{\Gamma_c} (u - u_h)\phi \, ds + a(u, v_h + \xi) - a(u_h, v_h) - \langle g, v_h + \xi - v_h \rangle_{\Gamma_s} \\ &= \int_{\Gamma_c} (u - u_h)\phi \, ds + a(u, \xi) + a(u - u_h, v_h - z) + a(u - u_h, z) \\ &\qquad - \langle g, \xi \rangle_{\Gamma_s}. \end{aligned} \tag{15}$$

Now using the fact that ξ satisfies (12a)–(12b) and integrating by parts, we deduce that

$$\begin{aligned} a(u, \xi) &= \int_{\Omega_1} \nabla u \nabla \xi - k^2 u \xi \, dA + \int_{\Omega_2} \nabla u \nabla \xi - k^2 u \xi \, dA - ik \int_{\Gamma_{inf}} u \xi \, ds \\ &= \int_{\partial \Omega_1} u \frac{\partial \xi}{\partial \nu_1} \, ds + \int_{\partial \Omega_2} u \frac{\partial \xi}{\partial \nu_2} \, ds - ik \int_{\Gamma_{inf}} u \xi \, ds; \end{aligned}$$

here ν_1 is the outward normal to Ω_1 and ν_2 is the outward normal to Ω_2. However, u and $\partial \xi / \partial \nu$ are continuous across Γ_c, so the contributions of the boundary integrals along Γ_c vanish. In addition ξ satisfies (12e) and (12f), which allows us to cancel integrals on Γ_s and Γ_{inf}. Thus

$$a(u, \xi) = 0. \tag{16}$$

Next we analyze $a(u-u_h,z)$. Using the fact that z satisfies (13a) and (13b) in the respective subdomains and integrating by parts, we obtain

$$\begin{aligned} a(u-u_h,z) &= \int_{\Omega_1} \nabla(u-u_h)\nabla z - k^2(u-u_h)z\,dA \\ &\quad + \int_{\Omega_2} \nabla(u-u_h)\nabla z - k^2(u-u_h)z\,dA - ik\int_{\Gamma_{inf}} (u-u_h)z\,ds \\ &= \int_{\partial\Omega_1} (u-u_h)\frac{\partial z}{\partial \nu_1}\,ds + \int_{\partial\Omega_2} (u-u_h)\frac{\partial z}{\partial \nu_2}\,ds \\ &\quad -ik\int_{\Gamma_{inf}} (u-u_h)z\,ds. \end{aligned}$$

However, $u-u_h$ is continuous across Γ_c and $[\partial z/\partial\nu]=\phi$, so there is a contribution from the boundary integrals along Γ_c. In addition z satisfies (13e) and (13f), which allows us to cancel integrals on Γ_s and Γ_{inf}. Thus

$$a(u-u_h,z) = -\int_{\Gamma_c} (u-u_h)\phi\,ds. \tag{17}$$

Using (16) and (17) in (15) proves the theorem. □

3.1. A priori estimates. Suppose that S_h consists of continuous piecewise p-degree polynomials or their curvilinear analogues on a regular triangulation of Ω. For each element K let h_K be the diameter of K (the diameter of the smallest circumscribed circle). Using the analysis of Schatz [23], problem (9) is known to have a unique solution for all sufficiently small h, and if the data are smooth enough,

$$||u-u_h||_{0,\Omega} + h^{1/2}||u-u_h||_{0,\Gamma_{inf}} + h||u-u_h||_{1,\Omega} \le Ch^{p+1}\|g\|_{p-1/2,\Gamma_s}. \tag{18}$$

We choose ψ_h to be the interpolant of ψ (for spaces with $p>1$ we use the interpolant defined by the endpoints and moments on each subinterval of the mesh on Γ_c, as in [10]).

THEOREM 3.2. *Assuming that ϕ and ψ are given by* (3) *and that $g\in H^{p-1}(\Gamma_s)$, the following a priori estimate holds for the computed far-field pattern:*

$$|u_\infty - u_{\infty,h}| \le C\left\{h^p\|u-u_h\|_{1,\Omega} + h^{p+1/2}\|u-u_h\|_{0,\Gamma_{inf}} + \|\psi-\psi_h\|_{-p+1,\Gamma_c}\right\}. \tag{19}$$

Remark. This theorem explains the frequently observed fact that the computed far-field pattern can be much more accurate than the field used to compute it.

COROLLARY 3.3. *Under the conditions of Theorem* 3.2 *and assuming $g\in H^{p-1/2}(\Gamma_s)$, if u_h satisfies the error estimates of* (18) *and if ψ_h is chosen to be the Blair interpolant of $\psi\in H^{p+1}(\Gamma_c)$* [10], *then*

$$|u_\infty - u_{\infty,h}| = O(h^{2p}).$$

Proof of Theorem 3.2. Using Theorem 3.1, the Cauchy–Schwarz inequality, and the fact that g is arbitrarily smooth on Γ_s gives

$$\begin{aligned} |u_\infty - u_{\infty,h}| \le{}& \|g\|_{p-1,\Gamma_s}\|\xi\|_{-p+1,\Gamma_s} + \|u-u_h\|_{1,\Omega_1}\|v_h-z\|_{1,\Omega_1} \\ &+\|u-u_h\|_{1,\Omega_2}\|v_h-z\|_{1,\Omega_2} \\ &+k\|u-u_h\|_{0,\Gamma_{inf}}\|v_h-z\|_{0,\Gamma_{inf}}. \end{aligned} \tag{20}$$

Now we choose v_h to be the interpolant of z in Ω_1 and Ω_2 using moment interpolation on Γ_c (so $[v_h] = \phi_h$), and since z is smooth in each subdomain (see subsection A.1),

$$\|v_h - z\|_{j,\Omega_1} + \|v_h - z\|_{j,\Omega_2} = O(h^{p+1-j}) \quad \text{for } j = 0, 1,$$

and so using the multiplicative trace inequality,

$$\|v_h - z\|_{0,\Gamma_{inf}} \leq C\|v_h - z\|_{0,\Omega}^{1/2}\|v_h - z\|_{1,\Omega}^{1/2} = O(h^{p+1/2}).$$

From the a priori estimates for ξ in subsection A.1 we obtain

$$\|\xi\|_{-p+1,\Gamma_s} \leq C\|\psi - \psi_h\|_{-p+1,\Gamma_c}.$$

Using these estimates in (20) we obtain the stated result. □

Proof of Corollary 3.3. Using the estimate (18) in (19) we obtain

$$|u_\infty - u_{\infty,h}| \leq C\left\{\|\psi - \psi_h\|_{-p+1,\Gamma_c} + O(h^{2p})\right\}.$$

Since we pick ψ_h to be the interpolant defined by pointwise interpolation at the ends of subintervals of the mesh on Γ_c and by suitable moments along the edges (see [10]), we obtain

$$\|\psi - \psi_h\|_{-p+1,\Gamma_c} = O(h^{2p}).$$

Thus we obtain the estimate in the corollary. □

3.2. A posteriori estimates. This section is devoted to proving an a posteriori error estimate for the far-field pattern. We shall state our result in various forms; the first result includes explicit expressions for the constants in the formula. These constants are defined next.

Interpolation constants: Let $w \in H^{p+1}(\Omega)$ and let $w_h \in S_h$ be the interpolant of w. Then on each triangle K in the mesh there are constants $C_{i,K}^{(0)}$ and $C_{i,K}^{(1)}$, independent of w, such that

$$\|w - w_h\|_{0,K} \leq C_{i,K}^{(0)} h_K^{p+1}\|w\|_{p+1,K},$$
$$\|w - w_h\|_{1,K} \leq C_{i,K}^{(1)} h_K^{p}\|w\|_{p+1,K}.$$

These interpolation constants can, in principle, be estimated for any given triangle shape (see [16] for linear triangles).

Generalized interpolation constants: Since we shall need to use the generalized interpolant, we need constants appearing in the estimates for this interpolant. For any triangle K we let $S(K)$ denote the union of all triangles touching K (either along edges or at vertices). Let $w \in H^1(\Omega)$ and let $w_h^{(e)} \in S_h$ be the Scott–Zhang generalized interpolant of w (see [11]). Then on each triangle K in the mesh there are constants $C_{i,K}^{(e,0)}$ and $C_{i,K}^{(e,1)}$, independent of w, such that

$$\|w - w_h\|_{0,K} \leq C_{i,K}^{(e,0)} h_K\|w\|_{1,S(K)},$$
$$\|w - w_h\|_{1,K} \leq C_{i,K}^{(e,1)}\|w\|_{1,S(K)}.$$

In principle the methods of [16] could be extended to compute approximations to these coefficients once the generalized interpolant is defined. Finally, we define C_s to

be the maximum number of triangles in $S(K)$ for all K (this is the maximum number of neighbors of a triangle).

Trace inequality constant: Let e be an edge of a triangle K_e and let $u \in H^1(K_e)$. We use the following trace inequality:

$$\|u\|_{0,e} \le C_e \left(h_{K_e}^{1/2} \|\nabla u\|_{0,K_e} + h_{K_e}^{-1/2} \|u\|_{0,K_e} \right). \tag{21}$$

This inequality is proved in Appendix B, where it is shown that $C_e \le \sqrt{3\delta_{K_e}}$, where δ_{K_e} measures the regularity of the mesh and is defined (for any triangle K) by

$$\frac{h_K}{\rho_K} = \delta_K.$$

Note that the regularity assumption implies $\delta_K \le \delta$ for all K.

THEOREM 3.4. *Let z_s solve* (13a)–(13f) *with $f = \psi$ and let ξ solve* (12a)–(12f). *Then under the conditions on the domain outlined previously, and using degree-p finite elements as in the previous section, we have the following a priori estimate, where the constants are independent of u and h:*

$$\begin{aligned}
|u_\infty - u_{\infty,h}| &\le \|g\|_{0,\Gamma_s} \|\xi\|_{0,\Gamma_s} + \sum_K \eta_K \|z_s\|_{p+1,K} + \sum_e \eta_e \|z_s\|_{p+1,K_e} \\
&\quad + \sum_K \mu_K \|\xi\|_{1,K} + \sum_e \mu_e \|\xi\|_{1,S(K_e)} \\
&\le \|g\|_{0,\Gamma_s} \|\xi\|_{0,\Gamma_s} + \left(\sum_K \eta_K^2 \right)^{1/2} \|z_s\|_{p+1,\Omega_1 \cup \Omega_2} + 3 \left(\sum_e \eta_e^2 \right)^{1/2} \|z_s\|_{p+1,\Omega_1 \cup \Omega_2} \\
&\quad + \left(\sum_K \mu_K^2 \right)^{1/2} \|\xi\|_{1,\Omega_1 \cup \Omega_2} + 3C_s \left(\sum_e \mu_e^2 \right)^{1/2} \|\xi\|_{1,\Omega_1 \cup \Omega_2},
\end{aligned}$$

where

$$\eta_K = C_{i,K}^{(0)} h_K^{p+1} \|\Delta u_h + k^2 u_h\|_{0,K},$$

$$\eta_e = \begin{cases} C_e (C_{i,K_e}^{(0)} + C_{i,K_e}^{(1)}) h_{K_e}^{p+1/2} \|[\partial u_h / \partial \nu_e]\|_{0,e} & \text{if } e \in \Omega, \\ C_e (C_{i,K_e}^{(0)} + C_{i,K_e}^{(1)}) h_{K_e}^{p+1/2} \|\partial u_h / \partial \nu - g\|_{0,e} & \text{if } e \in \Gamma_s, \\ C_e (C_{i,K_e}^{(0)} + C_{i,K_e}^{(1)}) h_{K_e}^{p+1/2} \|\partial u_h / \partial \nu - iku_h\|_{0,e} & \text{if } e \in \Gamma_{inf}, \end{cases}$$

$$\mu_K = C_{i,K}^{(e,0)} h_{K_e} \|\Delta u_h + k^2 u_h\|_{0,K},$$

$$\mu_e = \begin{cases} C_e (C_{i,K_e}^{(e,0)} + C_{i,K_e}^{(e,1)}) h_{K_e}^{1/2} \|[\partial u_h / \partial \nu_e]\|_{0,e} & \text{if } e \in \Omega, \\ C_e (C_{i,K_e}^{(e,0)} + C_{i,K_e}^{(e,1)}) h_{K_e}^{1/2} \|\partial u_h / \partial \nu - g\|_{0,e} & \text{if } e \in \Gamma_s, \\ C_e (C_{i,K_e}^{(e,0)} + C_{i,K_e}^{(e,1)}) h_{K_e}^{1/2} \|\partial u_h / \partial \nu - iku_h\|_{0,e} & \text{if } e \in \Gamma_{inf}. \end{cases}$$

Remark. All the constants in the above formula are known or can be estimated for a particular grid. The norms of z_s and ξ appearing in the bound can be estimated by noting that both functions are independent of the solution u and hence approximations to them can be computed. Note that ξ depends on the mesh size since it is computed from the difference between ψ and ψ_h on Γ_c (which is a priori known). An alternative to this computational approach is to use the well-posedness of the problems (12a)–(12f) and (13a)–(13f) to obtain bounds on the norms of z_s and ξ in terms of ψ and $\psi - \psi_h$. This route is pursued in Corollary 3.5 below.

Proof. Using Theorem 3.1,

$$u_\infty - u_{\infty,h} = -\int_{\Gamma_s} g\xi \, ds + a(u - u_h, v_h - z),$$

where z satisfies (13a)–(13f) with $f = \psi_h$. Note that $v_h - z$ does not jump across Γ_c (the jumps cancel—this is why we must choose $[z] = \psi_h$ on Γ_c) and hence $v_h - z \in H^1(\Omega)$. Thus, by (6),

$$a(u, v_h - z) = \langle g, v_h - z \rangle_{\Gamma_s}.$$

Let K represent a generic element in the mesh. Then, using the above equality,

$$\begin{aligned}
a(u - u_h, v_h - z) &= -\int_{\Omega_1} \nabla u_h \nabla(v_h - z) - k^2 u_h (v_h - z)\, dA \\
&\quad - \int_{\Omega_2} \nabla u_h \nabla(v_h - z) - k^2 u_h (v_h - z)\, dA \\
&\quad + ik \int_{\Gamma_{inf}} u_h (v_h - z)\, ds + \int_{\Gamma_s} g(v_h - z)\, ds \\
&= -\sum_{K \subset \Omega_1} \int_K \nabla u_h \nabla(v_h - z) - k^2 u_h (v_h - z)\, dA \\
&\quad - \sum_{K \subset \Omega_2} \int_K \nabla u_h \nabla(v_h - z) - k^2 u_h (v_h - z)\, dA \\
&\quad + ik \int_{\Gamma_{inf}} u_h (v_h - z)\, ds + \int_{\Gamma_s} g(v_h - z)\, ds.
\end{aligned}$$

Now integrating by parts on each element,

$$\begin{aligned}
&a(u - u_h, v_h - z) \\
&\quad = \sum_{K \subset \Omega_1} \left\{ \int_K (\Delta u_h + k^2 u_h)(v_h - z)\, dA - \int_{\partial K} \frac{\partial u_h}{\partial \nu_K} (v_h - z)\, ds \right\} \\
&\qquad + \sum_{K \subset \Omega_2} \left\{ \int_K (\Delta u_h + k^2 u_h)(v_h - z)\, dA - \int_{\partial K} \frac{\partial u_h}{\partial \nu_K} (v_h - z)\, ds \right\} \\
&\qquad + ik \int_{\Gamma_{inf}} u_h (v_h - z)\, ds + \int_{\Gamma_s} g(v_h - z)\, ds.
\end{aligned}$$

By choosing a normal ν_e to each edge in the mesh ($\nu_e = \nu$ on each of the three curves Γ_c, Γ_s, and Γ_{inf}) together with a consistent jump $[\cdot]_e$ for functions across each edge, we may rewrite the triangle edge contributions as integrals over edges and obtain

$$\begin{aligned}
&a(u - u_h, v_h - z) \\
&\quad = \sum_K \int_K (\Delta u_h + k^2 u_h)(v_h - z)\, dA + \sum_{e \in \Omega} \int_e \left[\frac{\partial u_h}{\partial \nu_e} \right]_e (v_h - z)\, ds \\
&\qquad + \sum_{e \in \Gamma_s} \int_e \left(g - \frac{\partial u_h}{\partial \nu} \right) (v_h - z)\, ds + \sum_{e \in \Gamma_{\text{inf}}} \int_e \left(iku_h - \frac{\partial u_h}{\partial \nu} \right) (v_h - z)\, ds.
\end{aligned}$$

Using the Cauchy–Schwarz inequality we obtain

$$
\begin{aligned}
&|a(u-u_h, v_h - z)| \\
&\leq \sum_K \|\Delta u_h + k^2 u_h\|_{0,K} \|v_h - z\|_{0,K} + \sum_{e\in\Omega} \left\| \left[\frac{\partial u_h}{\partial \nu_e} \right]_e \right\|_{0,e} \|v_h - z\|_{0,e} \\
&\quad + \sum_{e\in\Gamma_s} \left\| g - \frac{\partial u_h}{\partial \nu} \right\|_{0,e} \|v_h - z\|_{0,e} + \sum_{e\in\Gamma_{inf}} \left\| iku_h - \frac{\partial u_h}{\partial \nu} \right\|_{0,e} \|v_h - z\|_{0,e}. \qquad (22)
\end{aligned}
$$

Now we define $z_s = z + \xi$ and note that z_s satisfies (13a)–(13f) with $f = \psi$, and hence z_s is smooth (in Ω_1 and Ω_2). Thus we can estimate the first term on the right-hand side of (22) as

$$
\begin{aligned}
&\sum_K \|\Delta u_h + k^2 u_h\|_{0,K} \|v_h - z\|_{0,K} \\
&\leq \sum_K \|\Delta u_h + k^2 u_h\|_{0,K} \left(\|z_h - z_s\|_{0,K} + \|\xi_h - \xi\|_{0,K} \right),
\end{aligned}
$$

where z_h is the interpolant of z_s defined on Ω_1 and Ω_2 and ξ_h is the corresponding generalized interpolant of ξ (see [11]). Using the error estimates for these interpolants we obtain

$$
\begin{aligned}
&\sum_K \|\Delta u_h + k^2 u_h\|_{0,K} \|v_h - z\|_{0,K} \\
&\leq \sum_K \|\Delta u_h + k^2 u_h\|_{0,K} \left(C^{(0)}_{i,K} h_K^{p+1} \|z_s\|_{p+1,K} + C^{(e,0)}_{i,K} h_K \|\xi\|_{1,S(K)} \right). \qquad (23)
\end{aligned}
$$

We proceed similarly for the edge terms. First we estimate $\|v_h - z\|_{0,e}$. Let K_e be a triangle containing edge e. Then, using (21),

$$
\|v_h - z\|_{0,e} \leq C_e \left(h_{K_e}^{-1/2} \|v_h - z\|_{0,K_e} + h_{K_e}^{1/2} \|\nabla(v_h - z)\|_{0,K_e} \right).
$$

However, applying the interpolation error estimates,

$$
\begin{aligned}
h_{K_e}^{-1/2} \|v_h - z\|_{0,K_e} &\leq h_{K_e}^{-1/2} (\|z_h - z_s\|_{0,K_e} + \|\xi_h - \xi\|_{0,K_e}) \\
&\leq C^{(0)}_{i,K_e} h_{K_e}^{p+1/2} \|z_s\|_{p+1,K_e} + C^{(e,0)}_{i,K_e} h_{K_e}^{1/2} \|\xi\|_{1,K_e}.
\end{aligned}
$$

Similarly,

$$
h_{K_e}^{1/2} \|\nabla(v_h - z)\|_{0,K_e} \leq C^{(1)}_{i,K_e} h_{K_e}^{p+1/2} \|z_s\|_{p+1,K_e} + C^{(e,1)}_{i,K_e} h_{K_e}^{1/2} \|\xi\|_{1,K_e}.
$$

Using these estimates shows that

$$
\begin{aligned}
&\sum_{e\in\Omega} \left\| \left[\frac{\partial u_h}{\partial \nu_e} \right] \right\|_{0,e} \|v_h - z\|_{0,e} \\
&\leq \sum_{e\in\Omega} \left\| \left[\frac{\partial u_h}{\partial \nu_e} \right] \right\|_{0,e} C_e \left(h_{K_e}^{-1/2} \|v_h - z\|_{0,K_e} + h_{K_e}^{1/2} \|\nabla(v_h - z)\|_{0,K_e} \right) \\
&\leq \sum_{e\in\Omega} \left\| \left[\frac{\partial u_h}{\partial \nu_e} \right] \right\|_{0,e} C_e \left((C^{(0)}_{i,K_e} + C^{(1)}_{i,K_e}) h_{K_e}^{p+1/2} \|z_s\|_{p+1,K_e} \right. \\
&\qquad \left. + \left(C^{(e,0)}_{i,K_e} + C^{(e,1)}_{i,K_e} \right) h_{K_e}^{1/2} \|\xi\|_{1,S(K_e)} \right).
\end{aligned}
$$

The remaining terms in (22) are bounded in the same way.

The first estimate of the theorem is completed by writing

$$\left| \int_{\Gamma_s} g\xi \, ds \right| \leq \|g\|_{0,\Gamma_s} \|\xi\|_{0,\Gamma_s}.$$

The second estimate of the theorem is proved using the Cauchy–Schwarz inequality. The factor 3 and C_s are upper bounds on the number of times that a triangle is counted in estimating norms on the edges. □

Theorem 3.4 involves norms of z_s and ξ. The a posteriori estimate can be further simplified by using the well-posedness estimates for z_s and ξ proved in Appendix A.

COROLLARY 3.5. *Let z_s solve* (13a)–(13f) *with $f = \psi$ and let ξ solve* (12a)–(12f). *Then, under the conditions on the domain outlined previously, and using degree-p finite elements as in the previous section, we have the following a posteriori estimate, where the constants are independent of u and h:*

$$\begin{aligned} |u_\infty - u_{\infty,h}| \leq{}& C_{\xi,s} \|g\|_{0,\Gamma_s} \|\psi - \psi_h\|_{0,\Gamma_c} \\ &+ C_z \|\psi\|_{p+1,\Omega_1} \left\{ \left(\sum_K \eta_K^2 \right)^{1/2} + 3 \left(\sum_e \eta_e^2 \right)^{1/2} \right\} \\ &+ C_\xi \left[\left(\sum_K \mu_K^2 \right)^{1/2} + 3C_s \left(\sum_e \mu_e^2 \right)^{1/2} \right] \|\psi - \psi_h\|_{1/2,\Gamma_c}, \end{aligned} \tag{24}$$

where η_K, η_e, μ_K, and μ_e are as defined in Theorem 3.4. *The stability constants C_z, C_ξ, and $C_{\xi,s}$ are such that*

$$\begin{aligned} \|z_s\|_{p+1,\Omega_1 \cup \Omega_2} &\leq C_z \|\psi\|_{p+1,\Omega_1}, \\ \|\xi\|_{1,\Omega_1 \cup \Omega_2} &\leq C_\xi \|\psi - \psi_h\|_{1/2,\Gamma_c}, \\ \|\xi\|_{0,\Gamma_s} &\leq C_{\xi,s} \|\psi - \psi_h\|_{0,\Gamma_c}. \end{aligned}$$

Remark. The practical difficulty with this a posteriori bound is that the stability constants are difficult to estimate and depend on the wavenumber k. This aspect will be investigated further in the next section. The term $\|\psi - \psi_h\|_{1/2,\Gamma_c}$ can easily be estimated by function-space interpolation as follows:

$$\|\psi - \psi_h\|_{1/2,\Gamma_c}^2 \leq C \|\psi - \psi_h\|_{0,\Gamma_c} \|\psi - \psi_h\|_{1,\Gamma_c}.$$

4. Numerical results. Here we present some computational results, obtained using a cubic isoparametric finite element code (so $p = 3$). This code does not fit the curved boundaries exactly (as assumed in the theoretical sections) but uses the more convenient isoparametric technique.

One way that the a posteriori error estimate can be used is to provide *error indicators* for mesh refinement. The goal is to refine the mesh in a rational way but not to obtain a precise estimate of the error. This can be done as follows. We simply use (24), factoring out all the constants. As a further simplification we neglect the terms in the error indicator involving μ_K and μ_e, since we assume that ψ has already been well approximated on Γ_c by the initial mesh so that these terms are expected to be small. Factoring out the constants, we associate with element K the following indicator:

$$\gamma_K^2 = \eta_K^2 + \sum_{e \in K} \eta_e^2,$$

where we now take

$$\eta_K = h_K^{p+1} \|\Delta u_h + k^2 u_h\|_{0,K},$$

$$\eta_e = \begin{cases} h_K^{p+1/2} \|[\partial u_h/\partial \nu_e]\|_{0,e} & \text{if } e \in \Omega, \\ h_K^{p+1/2} \|\partial u_h/\partial \nu - g\|_{0,e} & \text{if } e \in \Gamma_s, \\ h_K^{p+1/2} \|\partial u_h/\partial \nu - iku_h\|_{0,e} & \text{if } e \in \Gamma_{inf}. \end{cases}$$

The algorithm seeks to equally distribute the error indicators below a given tolerance ϵ. After computing a finite element solution u_h, the error indicator γ_K is evaluated for each triangle. The error indicators are then used to flag triangles with a local indicator higher than the area-weighted tolerance proportional to ϵ. A red-green mesh subdivision strategy is used to refine the grid (with the restriction that adjacent triangles must be at most one level apart in refinement so that the grid remains regular) [6]. The algorithm continues until all indicators are below the required area-weighted value so that the final sum of the residuals is usually well below ϵ.

The first example approximates scattering from a circular scatterer and is useful because the exact solution can be computed using special function techniques.

4.1. A circular scatter. In this example we choose the domain Ω to be the annulus

$$\Omega = \left\{ \boldsymbol{x} \in \mathbb{R}^2 \mid 1 \leq |\boldsymbol{x}| \leq 3 \right\}.$$

The absorbing boundary (Γ_{inf}) is the outer boundary (circle of radius three), and the scatterer is the disk of radius one. The collection surface (Γ_c) is taken, arbitrarily, to be the circle of radius two. The incoming wave is modeled by taking the boundary data to be

$$g = \frac{\partial}{\partial \nu} \exp(ikx).$$

With this choice of Ω and g, problem (4a)–(4c) can be solved exactly using a Fourier–Bessel series, and hence the far-field pattern predicted by (5) can be evaluated as a series.

Our first results are shown in Figure 2 for $k = 2\pi$. This wavenumber gives a wavelength of one for the incoming field (exactly the radius of the scatterer). In Figure 2a we show the starting triangulation overlaid on a density plot of the real part of the solution. There are approximately nine grid points per wavelength in this case so the far-field pattern shown in Figure 3a is reasonably accurate (a relative L_2-norm error of just 5.05% compared to the exact solution of the truncated problem). If we use a tolerance $\epsilon = 0.1$, the algorithm takes two refinement steps using the meshes shown in Figure 2b–c. In the first step all triangles are refined, but in the next step fewer triangles are refined as needed. The far-field pattern corresponding to Figure 2b is shown in Figure 3b. Thereafter the graphs of the far-field patterns overlie one another.

Our next results are for the circle and $k = 4\pi$ so the wavelength of the incident wave is 0.5. The initial grid is no longer able to resolve the wave well (there are approximately 4.5 grid points per wavelength) and the far field computed with this grid is not accurate (see Figures 4a and 5a). Successive refinement steps improve the far-field pattern, but the final accuracy (a relative L_2-norm error of 0.21%) is worse than the final error achieved when $k = 2\pi$ and $\epsilon = 0.1$, indicating that the constant in our error formula increases with k.

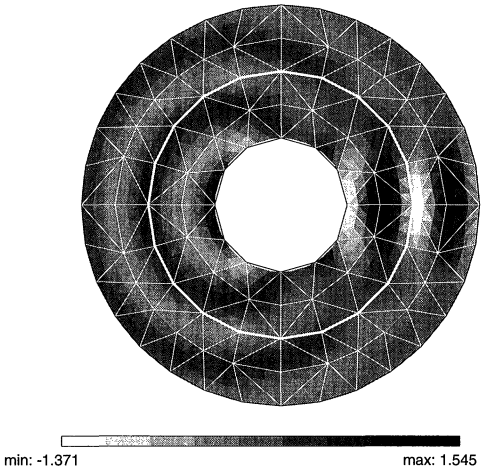

a) Initial mesh

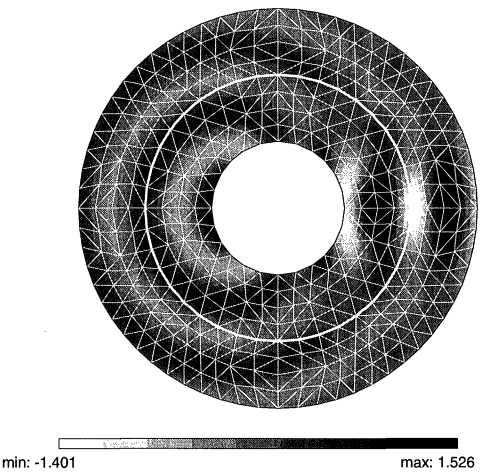

b) One step of refinement

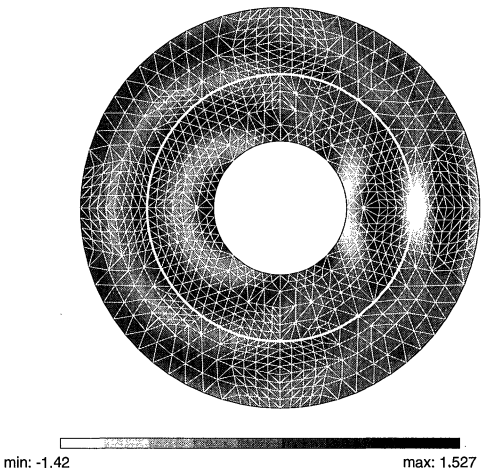

c) Final mesh

FIG. 2. *Here we show the results of the adaptive scheme with* $k = 2\pi$ *and* $\epsilon = 0.1$ *for the circular scatterer. We show the original coarse grid in* a) *followed by the successively refined grids. The grids are overlaid on a density plot of the real part of the finite element solution* u_h.

The main problem with the error indicator technique is that while it produces a sequence of grids that improve the far-field pattern, it does not provide a useful estimate of the actual error in the far-field pattern. We can evaluate the total indicator

$$\gamma = \left(\sum_K \gamma_K^2 \right)^{1/2}$$

and hope that it will be proportional to the error. Our proof estimate (3.4) shows (modulo the neglected terms) that for a given domain and wavenumber this is true. But even for a fixed domain, the constant of proportionality depends on the wavenumber k. To investigate the relationship we plot $\|u_\infty - u_{h,\infty}\|_0/\gamma$ for a range of k values in Figure 6. Clearly the ratio is increasing with k and in this case appears to increase

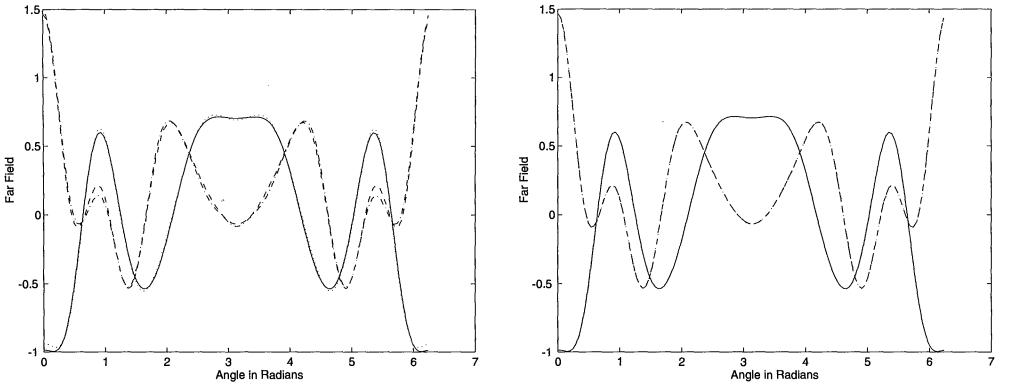

a) Initial mesh (error is 5.05%) b) One step of refinement (error is 0.12%)

FIG. 3. *Here we show the far-field patterns predicted by the adaptive scheme with* $k = 2\pi$ *and* $\epsilon = 0.1$ *for the circular scatterer. We show the real and imaginary parts of the true far field for the* truncated problem *(solid and long dashed lines) and the finite element result (dotted and dash-dot lines). The error reported is the relative* L_2*-error between the exact and finite element results for the truncated problem. After two steps of refinement (see Figure* 2c*) the final error is* 0.013%.

by $O(k^2)$. Given that $\|z_s\|_{4,\Omega_1\cup\Omega_2}$ is used in the a priori estimate we might have expected an $O(k^4)$ increase in the error, but for the range of k used here a quartic polynomial does not improve the fit appreciably. Our result does show that controlling the size of γ does not result in control of the error independent of k. Nevertheless the error indicators are useful for providing a means of refining the mesh.

4.2. A more complex example. In this section we apply the adaptive algorithm to a more complicated example. In this case we do not know the exact solution, and the problem is not covered by our theory since the scatterer is not smooth. Indeed the correct weighting of the residuals close to re-entrant corners needs to be investigated. The example is interesting because the scattered field is relatively small in certain directions from the scatterer, and hence a nonuniform mesh can provide a good approximation of the scattered field.

In this case the scatterer is contained in the box $-2 \leq x \leq 2.2$ and $-0.7 \leq y \leq 0.7$. The wavenumber is $k = 2\pi$ so the wavelength is one. The absorbing boundary condition is on the circle of radius five, and the collection surface is the circle of radius three.

The meshes used by the adaptive algorithm are shown in Figure 7, while the real part of the predicted far-field pattern is shown in Figure 8.

5. Conclusion. We have presented an analysis of the error in computing the far-field pattern of a scatterer using finite elements. A similar method can also be used for Maxwell's equations in three dimensions, and we will analyze this in a forthcoming paper.

Our numerical examples show that the error indicators can be used to refine the mesh and improve the estimated far-field pattern, but there is still much work to be done to provide reliable error estimates that are robust to changes in the parameter k. By computing an approximate solution of the adjoint problem (i.e., to z) we hope to be able to accomplish this in an efficient manner.

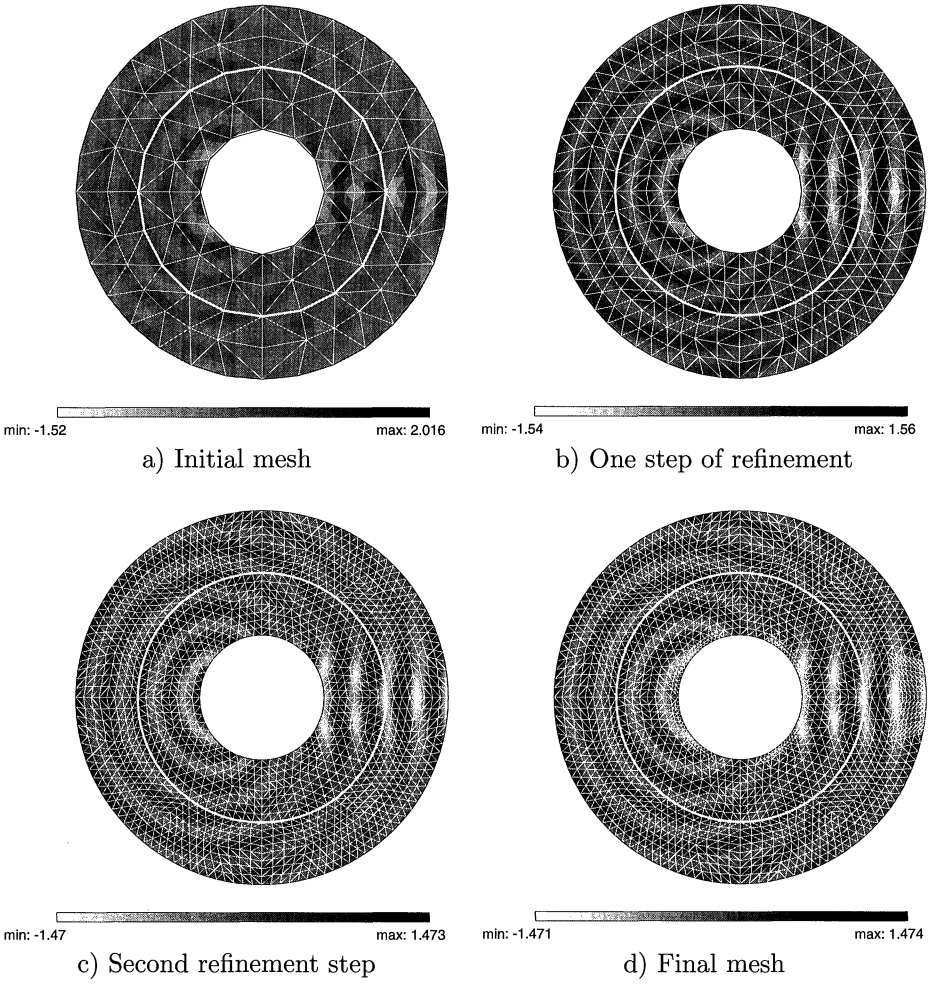

FIG. 4. *Here we show the results of the adaptive scheme with* $k = 4\pi$ *and* $\epsilon = 0.1$ *for the circular scatterer. We show the original coarse grid in* a) *followed by the successively refined grids. The grids are overlaid on a density plot of the real part of the finite element solution* u_h. *The coarse grid in* a) *is unable to resolve the field.*

Appendix A. Analysis of the transmission problem.

A.1. The general problem. In this section we study the existence, uniqueness, and regularity of the weak solution z to the following problem:

$$\Delta z + k^2 z = 0 \text{ in } \Omega_1, \tag{25a}$$

$$\Delta z + k^2 z = 0 \text{ in } \Omega_2, \tag{25b}$$

$$[z] = f \text{ on } \Gamma_c, \tag{25c}$$

$$\left[\frac{\partial z}{\partial \nu}\right] = g \text{ on } \Gamma_c, \tag{25d}$$

$$\frac{\partial z}{\partial \nu} = 0 \text{ on } \Gamma_s, \tag{25e}$$

$$\frac{\partial z}{\partial \nu} - ikz = 0 \text{ on } \Gamma_{inf}, \tag{25f}$$

where $f \in H^{1/2}(\Gamma_c)$ and $g \in H^{-1/2}(\Gamma_c)$ are given functions.

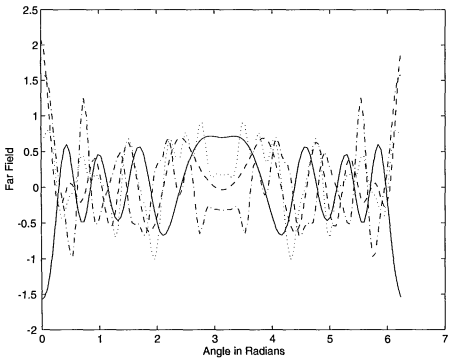

a) Initial mesh (error is 126%)

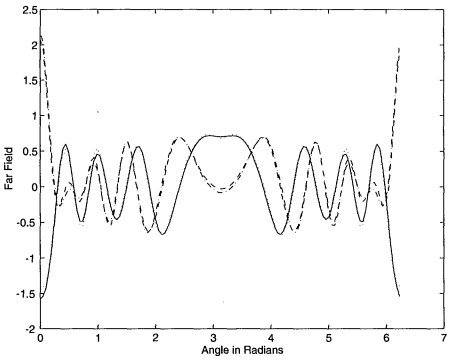

b) One step of refinement (error is 9.98%)

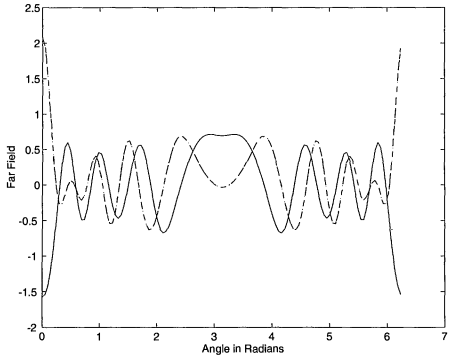

a) Second refinement step (error is 0.23%)

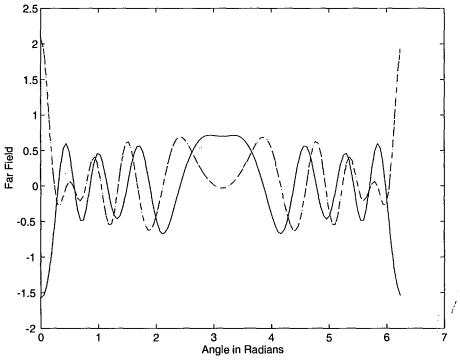

b) Final result (error is 0.21%)

FIG. 5. *Here we show the far-field patterns predicted by the adaptive scheme with* $k = 2\pi$ *and* $\epsilon = 0.1$ *for the circular scatterer. We show the real and imaginary parts of the true far field and the finite element result (see Figure* 3 *for definitions). The error reported is the relative* L_2*-error between the exact and finite element results for the truncated problem. Despite having the same truncation coefficient* $\epsilon = 0.1$ *as in the example in Figures* 2–3 *the final error obtained is nearly* 10 *times as large.*

First of all it is easy to see that this problem has at most one solution.

LEMMA A.1. *Problem* (25a)–(25f) *has at most one solution.*

Proof. When $f = g = 0$ in (25a)–(25f), the function z is the weak solution of

$$\begin{aligned} \Delta z + k^2 z &= 0 \text{ in } \Omega, \\ \frac{\partial z}{\partial \nu} &= 0 \text{ on } \Gamma_s, \\ \frac{\partial z}{\partial \nu} - ikz &= 0 \text{ on } \Gamma_{inf}, \end{aligned}$$

and this standard problem has a unique solution. □

Next we prove existence using the Fredholm alternative. The weak formulation of the problem involves the space

$$Z = \left\{ u \mid u|_{\Omega_1} \in H^1(\Omega_1),\ u|_{\Omega_2} \in H^1(\Omega_2),\ [u] = f \text{ on } \Gamma_c \right\}.$$

Then $z \in Z$ satisfies

$$a(z, v) = \langle g, v \rangle_{\Gamma_c} \text{ for all } v \in H^1(\Omega).$$

This is a transmission problem for the Helmholtz equation.

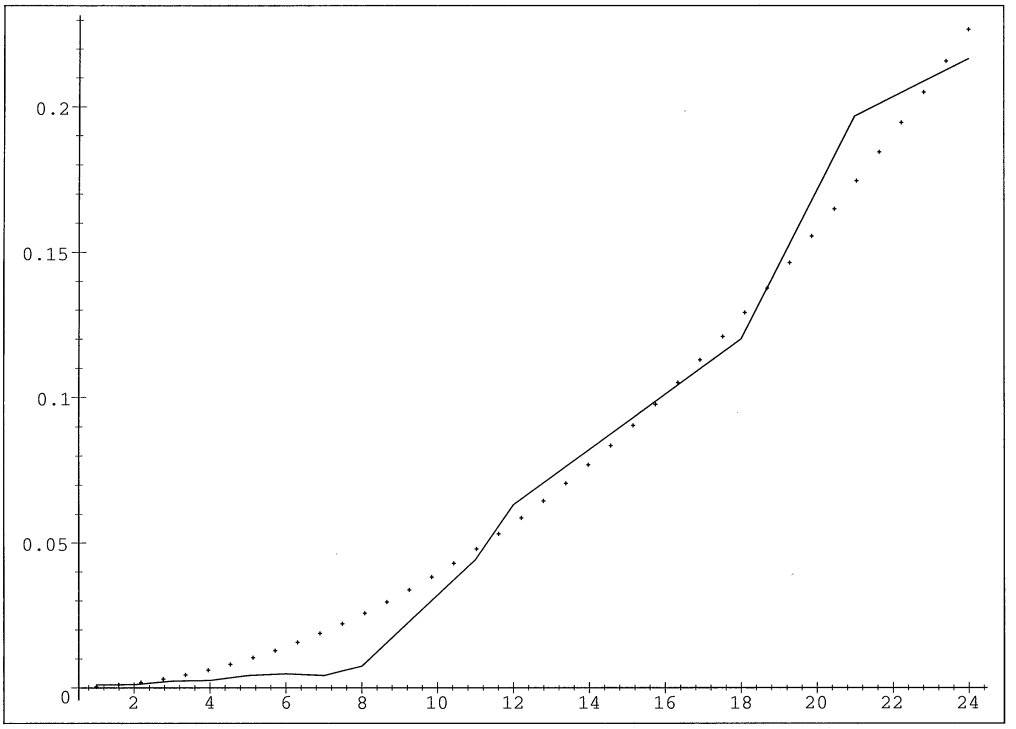

FIG. 6. *Here we plot* $\|u_\infty - u_{h,\infty}\|_0/\gamma$ *against* k *(solid line) and a best-fit pure quadratic polynomial (dotted line) for the circular scatterer. Clearly* $\|u_\infty - u_{h,\infty}\|_0 = O(k^2)\gamma$ *in this case, so control of* γ *does not control the far-field error independently of* k*. Here we chose* $\epsilon = 0.1$.

LEMMA A.2. *There exists a unique weak solution* $z \in Z$ *to* (25a)–(25f) *and*

$$\|z\|_{1,\Omega_1} + \|z\|_{1,\Omega_2} \leq C\left(\|f\|_{1/2,\Gamma_c} + \|g\|_{-1/2,\Gamma_c}\right).$$

Proof. Let $\tilde{f} \in H^1(\Omega_1)$ be any extension of f to Ω satisfying $\|\tilde{f}\|_{1,\Omega_1} \leq C\|f\|_{1/2,\Gamma_c}$ (for example, $\tilde{f}$ could satisfy $\Delta\tilde{f} = 0$ in Ω_1, $\tilde{f} = f$ on Γ_c, and $\tilde{f} = 0$ on Γ_s). In addition we define $\tilde{f} = 0$ on Ω_2, and introduce $\tilde{z} = z + \tilde{f}$. Note that

$$[\tilde{z}] = [z] + [\tilde{f}] = 0,$$

so $\tilde{z} \in H^1(\Omega)$ satisfies

$$a(\tilde{z}, v) = a(\tilde{f}, v) + \langle g, v\rangle_{\Gamma_c} \text{ for all } v \in H^1(\Omega).$$

To analyze this problem we write

$$a(\tilde{z}, v) = [a(\tilde{z}, v) + b(\tilde{z}, v)] - b(\tilde{z}, v),$$

where

$$b(\tilde{z}, v) = 2k^2 \int_\Omega \tilde{z}\, v\, dA.$$

Note that $a(z, \overline{w}) + b(z, \overline{w})$ is the natural inner product on $H^1(\Omega)$. Now define $B : H^1(\Omega) \to H^1(\Omega)$ by

$$a(B\tilde{z}, v) + b(B\tilde{z}, v) = b(\tilde{z}, v) \text{ for all } v \in H^1(\Omega).$$

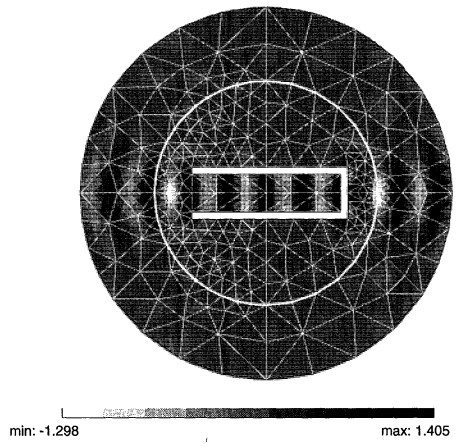

a) Initial mesh

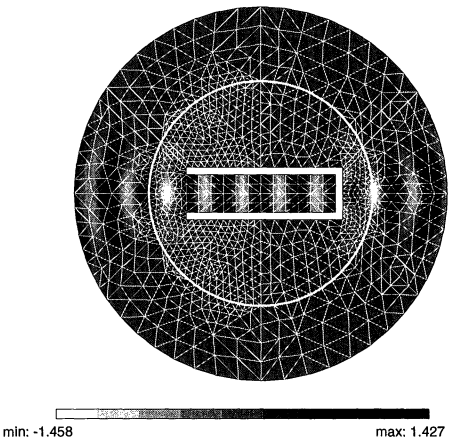

b) One step of refinement

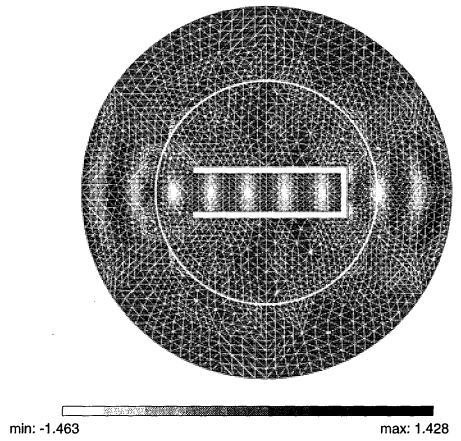

c) Second refinement step

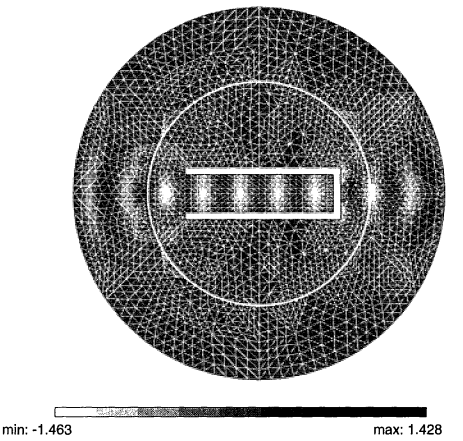

d) Final mesh

FIG. 7. *Here we show the results of the adaptive scheme with* $k = 2\pi$ *and* $\epsilon = 0.1$ *for the benchmark scatterer. We show the original coarse grid in* a) *followed by the successively refined grids. The grids are overlaid on a density plot of the real part of the finite element solution* u_h.

Then B is well defined and compact (since $H^1(\Omega)$ is compactly embedded in $L^2(\Omega)$). Finally, if we define $J \in H^1(\Omega)$ by

$$a(J, v) + b(J, v) = a(\tilde{f}, v) + \langle , v\rangle_{\Gamma_c} \text{ for all } v \in H^1(\Omega),$$

the weak form of the differential equation can be written as the operator equation

$$(I - B)\tilde{z} = J.$$

Using the Fredholm alternative theorem and the uniqueness of the solution z proves existence of the solution in Z. □

A.2. Problem (12a)–(12f). For problem (12a)–(12f), the multiplicative trace theorem and Lemma A.2 show the following result.

COROLLARY A.3. *There is a unique weak solution* ξ *of* (12a)–(12f) *and*

$$\|\xi\|_{1,\Omega_1} + \|\xi\|_{1,\Omega_2} + \|\xi\|_{1/2,\Gamma_s} \leq C\|\psi - \psi_h\|_{1/2,\Gamma_c}.$$

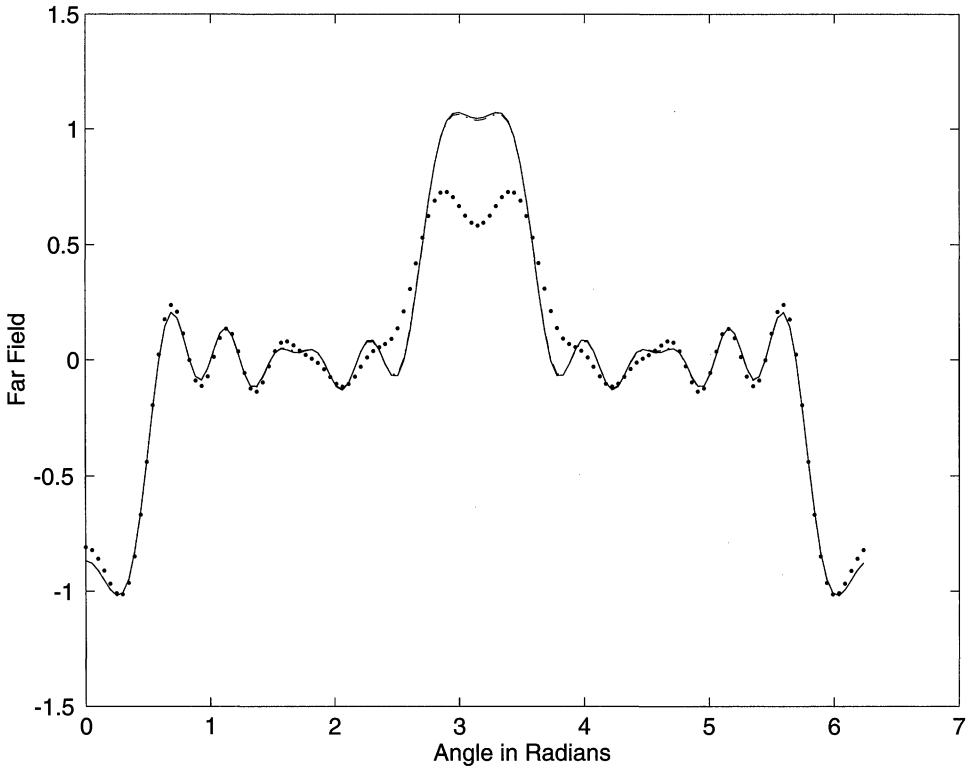

FIG. 8. *Here we show the real part of the far-field patterns predicted by the adaptive scheme with* $k = 2\pi$ *and* $\epsilon = 0.1$ *for the benchmark problem. The dotted line is the far-field pattern for the initial grid. The remaining three lines (which almost overlie one another) are the results for the remaining refinement steps.*

We also prove the following result relating norms of ξ on Γ_c to the data (i.e., to $\psi - \psi_h$).

LEMMA A.4. *For* $s < 1/2$ *there exists a constant* $C = C(s)$ *such that*

$$\|\xi\|_{s,\Gamma_s} \leq C\|\psi - \psi_h\|_{s,\Gamma_c}.$$

Proof. Let $\chi \in H^{-s}(\Gamma_s)$ and define $w \in H^{-s+3/2}(\Omega)$ to be the weak solution of

$$\begin{aligned} \Delta w + k^2 w &= 0 \text{ in } \Omega, \\ \frac{\partial w}{\partial \nu} &= \chi \text{ on } \Gamma_s, \\ \frac{\partial w}{\partial \nu} - ikw &= 0 \text{ on } \Gamma_{inf}. \end{aligned}$$

Then using the weak problem for ξ and integrating by parts,

$$\begin{aligned} 0 &= a(\xi, w) \\ &= \left\langle \xi, \frac{\partial w}{\partial \nu} \right\rangle_{\partial\Omega_1} + \left\langle \xi, \frac{\partial w}{\partial \nu} \right\rangle_{\partial\Omega_2} - ik\langle \xi, w \rangle_{\Gamma_{inf}} \\ &= \langle \xi, \chi \rangle_{\Gamma_s} - \left\langle [\xi], \frac{\partial w}{\partial \nu} \right\rangle_{\Gamma_c}. \end{aligned}$$

Hence

$$|\langle \xi, \chi \rangle_{\Gamma_s}| \leq \|[\xi]\|_{s,\Gamma_c} \left\| \frac{\partial w}{\partial \nu} \right\|_{-s,\Gamma_c}.$$

Noting that Ω is a domain with a C^∞ boundary, the following a priori estimate holds for $s < 1/2$:

$$\left\| \frac{\partial w}{\partial \nu} \right\|_{-s,\Gamma_c} \leq C \|\chi\|_{-s,\Gamma_s}.$$

Combining the last two inequalities and recalling the definition of the dual norm complete the proof. □

A.3. A special case of problem (25a)–(25f). Here we will study problem (25a)–(25f) in the special case when $f = \psi$ and $g = \phi$, where ϕ and ψ are given by (3). In this case (25a)–(25f) is particularly simple to analyze and approximate because ψ satisfies the Helmholtz equation as a function of $\boldsymbol{y}$ and

$$\phi = \frac{\partial \psi}{\partial \nu}.$$

Thus, if we define w by

$$w(\boldsymbol{x}) = \begin{cases} z(\boldsymbol{x}) + \psi(\hat{\boldsymbol{x}}, \boldsymbol{x}) & \text{if } \boldsymbol{x} \in \Omega_1, \\ z(\boldsymbol{x}) & \text{if } \boldsymbol{x} \in \Omega_2, \end{cases}$$

then w satisfies the Helmholtz equation in Ω_1 and Ω_2 together with the homogeneous boundary conditions (25f). On Γ_c,

$$[w] = [z] - \psi = 0 \text{ and } \left[\frac{\partial w}{\partial \nu}\right] = \left[\frac{\partial z}{\partial \nu}\right] - \frac{\partial \psi}{\partial \nu} = 0,$$

while on Γ_s,

$$\frac{\partial w}{\partial \nu} = \frac{\partial z}{\partial \nu} + \frac{\partial \psi}{\partial \nu} = \frac{\partial \psi}{\partial \nu}.$$

Thus $w \in H^1(\Omega)$ is the weak solution of the standard problem

$$\Delta w + k^2 w = 0 \quad \text{in } \Omega, \tag{26a}$$

$$\frac{\partial w}{\partial \nu} = -\frac{\partial \psi}{\partial \nu} \quad \text{on } \Gamma_s, \tag{26b}$$

$$\frac{\partial w}{\partial \nu} - ikw = 0 \quad \text{on } \Gamma_{inf}. \tag{26c}$$

Notice that w is entirely independent of Γ_c so that the smoothness of z is independent of Γ_c. We have the following result.

LEMMA A.5. *For the special case of ϕ and ψ given by* (3), *there is a unique solution z to* (25a)–(25f) *given by*

$$z(\boldsymbol{x}) = \begin{cases} w(\boldsymbol{x}) - \psi(\hat{\boldsymbol{x}}, \boldsymbol{x}) & \text{if } \boldsymbol{x} \in \Omega_1, \\ w(\boldsymbol{x}) & \text{if } \boldsymbol{x} \in \Omega_2, \end{cases}$$

where w satisfies (26a)–(26c). *Furthermore, for any $s \geq 1$,*

$$\|z\|_{s,\Omega_1\cup\Omega_2} \leq C\left(\|\psi\|_{s,\Omega_1} + \left\|\frac{\partial\psi}{\partial\nu}\right\|_{s-3/2,\Gamma_s}\right).$$

This lemma gives us a simple way to compute approximations to z by approximating w.

Appendix B. A trace inequality. In this section we prove the following trace inequality taking care to estimate the constant.

LEMMA B.1. *Let e be an edge of a triangle K and let $u \in H^1(K)$. The following trace inequality holds:*

$$\|u\|_{0,e} \leq C_e\left(h_K^{1/2}\|\nabla u\|_{0,K} + h_K^{-1/2}\|u\|_{0,K}\right),$$

where $C_e \leq \sqrt{5\delta_K/2}$.

Proof. Consider the triangle with vertices $(0,0)$, $(a,0)$, and (b,c), where we assume $a > 0$ and $c > 0$. We will take e to be the edge connecting $(0,0)$ and $(a,0)$. Let $\boldsymbol{v}$ be defined by

$$\boldsymbol{v}(x,y) = \frac{1}{c}\begin{pmatrix} -b+x \\ -c+y \end{pmatrix}.$$

This function has the property that its normal component has magnitude one on e and vanishes on the other two edges of K. Furthermore,

$$\nabla\cdot\boldsymbol{v} = 2/c \text{ and } |\boldsymbol{v}|_{\infty,K} \leq \max\left(\frac{\sqrt{b^2+c^2}}{c}, \frac{\sqrt{(a-b)^2+c^2}}{c}\right).$$

Hence, since $\max(\sqrt{b^2+c^2}, \sqrt{(a-b)^2+c^2}) \leq h_K$ and $c > \rho_K$ we have that

$$|\boldsymbol{v}|_{\infty,K} \leq \frac{h_K}{\rho_K} = \delta_K.$$

(Obviously a better bound could be computed for a given triangle.)

Now using the divergence theorem and the Cauchy–Schwarz inequality we have

$$\begin{aligned}
\|u\|_{0,e}^2 &= \int_{\partial K} u^2\boldsymbol{v}\cdot\boldsymbol{\nu}\,ds \\
&= \int_K \nabla\cdot\left(u^2\boldsymbol{v}\right)\,dA \\
&= \int_K \left(2u\nabla u\cdot\boldsymbol{v} + u^2\nabla\cdot\boldsymbol{v}\right)\,dA \\
&\leq 2\int_K \left(|u||\nabla u|\|\boldsymbol{v}\|_{\infty,K} + \frac{1}{c}u^2\right)\,dA \\
&\leq \int_K \left(|\nabla u|^2\frac{\|\boldsymbol{v}\|_{\infty,K}}{\epsilon} + \left(\epsilon\|\boldsymbol{v}\|_{\infty,K} + \frac{2}{c}\right)u^2\right)\,dA
\end{aligned}$$

for any $\epsilon > 0$. Now we note that $1/c < 1/\rho_K \leq \delta_K/h_K$ and choose $\epsilon = h_K^{-1}/2$ to obtain

$$\|u\|_{0,e}^2 \leq \int_K \left(2h_K\delta_K|\nabla u|^2 + \frac{5\delta_K}{2h_K}u^2\right)\,dA.$$

Taking square roots of both sides completes the proof. □

REFERENCES

[1] M. AINSWORTH, D. KELLY, I. SLOAN, AND S. WANG, *Post-processing with computable error bounds for finite element approximation of a nonlinear heat conduction problem*, IMA J. Numer. Anal., 17 (1997), pp. 547–561.

[2] I. BABUŠKA AND A. MILLER, *The post-processing approach in the finite element method – Part 1: Calculation of displacements, stresses and other higher derivatives of the displacements*, Internat. J. Numer. Methods Engrg., 20 (1984), pp. 1085–1109.

[3] I. BABUŠKA AND A. MILLER, *The post-processing approach in the finite element method – Part 2: The calculation of stress intensity factors*, Internat. J. Numer. Methods Engrg., 20 (1984), pp. 1110–1129.

[4] I. BABUŠKA AND A. MILLER, *The post-processing approach in the finite element method – Part 3: A posteriori error estimates and adaptive mesh selection*, Internat. J. Numer. Methods Engrg., 20 (1984), pp. 2311–2324.

[5] I. BABUŠKA AND M. SURI, *The p and hp versions of the finite element method, basic principles and properties*, SIAM Rev., 36 (1994), pp. 578–632.

[6] R. BANK, *PLTMG User's Guide*, Tech. report edition 4.0, University of California, San Diego, 1985.

[7] J. BARRETT AND C. ELLIOTT, *Total flux estimates for a finite-element approximation of elliptic equations*, IMA J. Numer. Anal., 7 (1987), pp. 129–148.

[8] J. BERENGER, *A perfectly matched layer for the absorption of electromagnetics waves*, J. Comput. Phys., 114 (1994), pp. 185–200.

[9] C. BERNARDI, *Optimal finite element interpolation on curved domains*, SIAM J. Numer. Anal., 26 (1989), pp. 1212–1240.

[10] J. BLAIR, *Higher order approximations to the boundary conditions for the finite element method*, Math. Comput., 30 (1976), pp. 250–262.

[11] S. BRENNER AND L. SCOTT, *The Mathematical Theory of Finite Element Methods*, Springer-Verlag, New York, 1994.

[12] F. COLLINO, *High order absorbing boundary conditions for wave propagation models: Straight line boundary and corner cases*, in Second Internat. Conf. Mathematical and Numerical Aspects of Wave Propagation, R. Kleinman, et al., eds., SIAM, Philadelphia, 1994, pp. 161–171.

[13] D. COLTON AND R. KRESS, *Inverse Acoustic and Electromagnetic Scattering Theory*, Appl. Math. Sci. 93, Springer-Verlag, New York, 1991.

[14] M. GILES, M. LARSON, M. LEVENSTAM, AND E. SÜLI, *Adaptive Error Control for Finite Element Approximations of the Lift and Drag Coefficients in Viscous Flow*, Tech. report NA-97/06, Oxford University Computing Laboratory, Oxford, UK, 1997.

[15] C. GOLDSTEIN, *The finite element method with non-uniform mesh sizes applied to the exterior Helmholtz problem*, Numer. Math., 38 (1981), pp. 61–82.

[16] D. HANDSCOMB, *Errors of Linear Interpolation on a Triangle*, Tech. report 95/09, Oxford University Computing Laboratory, Oxford, UK, 1995.

[17] J.-M. JIN, *The Finite Element Method in Electromagnetics*, John Wiley, New York, 1993.

[18] J. KELLER AND D. GIVOLI, *Exact non-reflecting boundary conditions*, J. Comput. Phys., 82 (1989), pp. 172–192.

[19] A. KIRSCH AND P. MONK, *Convergence analysis of a coupled finite element and spectral method in acoustic scattering*, IMA J. Numer. Anal., 9 (1990), pp. 425–447.

[20] A. KIRSCH AND P. MONK, *An analysis of the coupling of finite element and Nyström methods in acoustic scattering*, IMA J. Numer. Anal., 14 (1994), pp. 523–544.

[21] M. LENOIR, M. VULLIERME-LEDARD, AND C. HAZARD, *Variational formulations for the determination of resonant states in scattering problems*, SIAM J. Math. Anal., 23 (1992), pp. 579–608.

[22] P. MONK, *The near field to far field transformation*, COMPEL, 14 (1995), pp. 41–56.

[23] A. SCHATZ, *An observation concerning Ritz-Galerkin methods with indefinite bilinear forms*, Math. Comp., 28 (1974), pp. 959–962.

[24] J. WHEELER, *Permafrost thermal design for the trans-Alaska pipeline*, in Moving Boundary Problems, D. Wilson, A. Solomon, and P. Boggs, eds., Academic Press, New York, 1978, pp. 267–284.